molecules

MDPI

Article

Controlled Synthesis of Au_{25} Superatom Using a Dendrimer Template

Hisanori Muramatsu [1], Tetsuya Kambe [1,2], Takamasa Tsukamoto [1,2,3], Takane Imaoka [1,2] and Kimihisa Yamamoto [1,2,*]

[1] Laboratory of Chemistry and Life Science (CLS), Tokyo Institute of Technology, Yokohama 226-8503, Japan; muramatsu.h.ae@m.titech.ac.jp (H.M.); kambe.t.aa@m.titech.ac.jp (T.K.); tsukamoto.t.ad@m.titech.ac.jp (T.T.); timaoka@res.titech.ac.jp (T.I.)
[2] JST-ERATO, Yamamoto Atom Hybrid Project, Tokyo Institute of Technology, Yokohama 226-8503, Japan
[3] JST-PRESTO, Kawaguchi 332-0012, Japan
* Correspondence: yamamoto.k.at@m.titech.ac.jp; Tel.: +81-45-924-5260

Abstract: Superatoms are promising materials for their potential in elemental substitution and as new building blocks. Thus far, various synthesis methods of thiol-protected Au clusters including an Au_{25} superatom have been investigated. However, previously reported methods were mainly depending on the thermodynamic stability of the aimed clusters. In this report, a synthesis method for thiol-protected Au clusters using a dendrimers template is proposed. In this method, the number of Au atoms was controlled by the stepwise complexation feature of a phenylazomethine dendrimer. Therefore, synthesis speed was increased compared with the case without the dendrimer template. Hybridization for the Au_{25} superatoms was also achieved using the complexation control of metals.

Keywords: superatoms; dendrimers; gold clusters

Citation: Muramatsu, H.; Kambe, T.; Tsukamoto, T.; Imaoka, T.; Yamamoto, K. Controlled Synthesis of Au_{25} Superatom Using a Dendrimer Template. *Molecules* **2022**, *27*, 3398. https://doi.org/10.3390/molecules27113398

Academic Editors: Lucian Baia, Klara Magyari and Jin Won (Maria) Seo

Received: 21 April 2022
Accepted: 19 May 2022
Published: 25 May 2022

1. Introduction

Some clusters consisting of a few to several dozen metal atoms can provide discrete atom-like electron states according to DFT calculations with the Jellium model [1,2]. Metal clusters with this property, called "superatoms," are attracting attention. Among them, a halogen superatom of Al_{13}^- [3] and an alkali-metal superatom of Cu_8^-/Ag_8^- [4] are well-known examples. In the latter case, electronegativity lower than the alkali metal elements (Li, Na, K, Rb, or Cs) is proposed, demonstrating a super-alkali superatom. Therefore, the development of synthesis methods for such superatoms has been a significant target of recent research.

Among these superatoms, Au clusters have been focused on as useful candidates for superatoms that can be synthesized not only in the gas phase but also in the solution phase [5,6]. Since the synthesis of thiol-protected Au clusters was reported by Brust and Schiffrin et al. [5], lots of research [6–29] has investigated them. Especially, $Au_{25}SR_{18}$ [30,31], $Au_{38}SR_{24}$ [6,32,33] and $Au_{144}SR_{60}$ [6,34,35] (R: hydrocarbons) are studied as superatomic clusters. They were purified and characterized by single crystal analysis [30,31]. In addition, the introduction of different elements, such as Pd, Pt, Cu, Ag, Cd, and Hg [23,24,27,28,36–39] into Au clusters has been reported. The mixing has been carried out by metal-exchanging. However, the synthesis of these materials often requires low-temperature conditions [30,40] or an etching reaction for several days [41] to increase the synthetic yields.

Dendrimer templates are attractive for the solution phase synthesis of metal clusters or particles since their sizes can be controlled in the state of the precursors [42–58]. One of the most famous dendrimers is the polyamidoamine (PAMAM) dendrimer, which is limited in accuracy for metal assembly due to its random complexation fashion. In contrast, phenylazomethine dendrimers enable atomicity control for cluster synthesis [59–69]. Some

clusters prepared by this method are found to exhibit high catalytic activities depending on the number of atoms. In addition, the specific high activity of a Pt_{17} catalyst is also reported [70]. Superatom synthesis using this phenylazomethine dendrimer has also been reported. The synthesis and properties of Al_{13}^- [71] and Ga_{13}^- [72] in the dendrimer were also demonstrated. In this study, we investigated dendrimer-templating synthesis for the thiol-protected Au_{25} superatom. As the template, a phenylazomethine dendrimer with a tetraphenyl methane core part (TPM G4) was used. Due to the metal-complexation feature of the TPM G4, one atom blending was also demonstrated.

2. Result and Discussion

2.1. Controlled Assembly of $AuCl_3$ on TPM G4

The TPM G4 has tetraphenylmethane in the core and a fourth-generation imine skeleton in the branches, with higher electron density in the inner layers (Figure S1). In order to use the TPM G4 as a precise template, metal salts and the imine parts of the TPM G4 are required to be connected by a 1:1 ratio. Based on the previous reports [65–69], the mixed solution of chloroform:acetonitrile = 1:1 was used as a solvent for the metal assembly. The stepwise coordination fashion between the dendrimer and $AuCl_3$ was confirmed by UV-Vis titration (Figure S2). Isosbestic points, according to the number of imines at each layer of the TPM G4, were observed during the addition of the acetonitrile solution of $AuCl_3$. The result indicates its 1:1 complexation. The observed isosbestic points at 336.5 nm (0~4 equiv.), 344.0 nm (4~12 equiv.), 332.0 nm (12~28 equiv.) and 328.0 nm (28~60 equiv.) indicate the stepwise coordination of the inner layer imines as shown in the Figure S2. These results indicate that the TPM G4 can be used as an accurate template for Au clusters.

The $Au_{25}PET_{18}$ superatom (PET: 2-phenylethanethiol: SCH_2CH_2Ph) was synthesized by adding thiol-ligand solution at the same time as the reduction of $AuCl_3$ in the TPM G4 (Figure 1). Though this method is similar to our previously reported methods [62,67,70,72], it is different due to the addition of the thiol ligands to protect the surface of Au clusters. In addition, the solvent of $NaBH_4$ was changed from methanol to ice-cold water. When $NaBH_4$/methanol solution was used, $Au_{25}PET_{18}$ was not obtained. After the reactions, the solution was stirred for 3 h. Then the solvent was removed using an evaporator after filtration. The obtained dark-brown solid was purified by washing with a water/methanol mixture, and the Au clusters were extracted with acetonitrile. The obtained solution was subjected to MALDI-TOF-MS measurement in linear mode (Figure 2a). As a result, the peak corresponding to $Au_{25}PET_{18}$ (m/z = 7390.73) was detected with the fragment peak of $[Au_{21}PET_{14}]^+$ (m/z = 6057.25) [73]. The calculated exact mass [74] of $Au_{25}PET_{18}$ (m/z = 7391.93) confirms the formation of the aimed superatom. UV-vis spectra of the synthesized $Au_{25}PET_{18}$ (Figure 2b) showed broad absorption from 800 nm to 600 nm and 450 nm indicating the formation of $Au_{25}PET_{18}$ [40,75–77]. The expected peak around 400 nm was unclear. This may be due to the overlap of the dendrimer absorption peaks with the peak top around 320 nm.

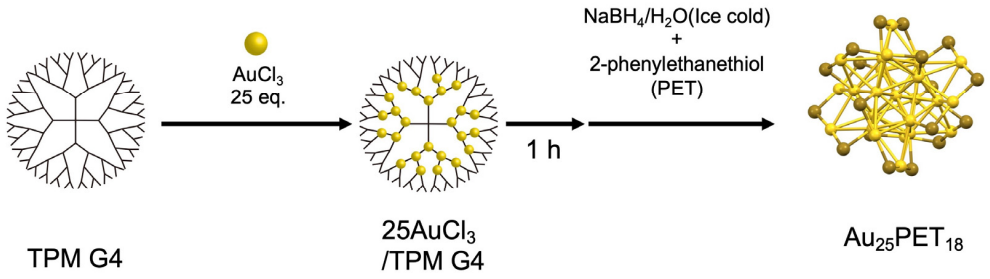

Figure 1. Synthetic scheme of an $Au_{25}PET_{18}$ superatom using the TPM G4 template.

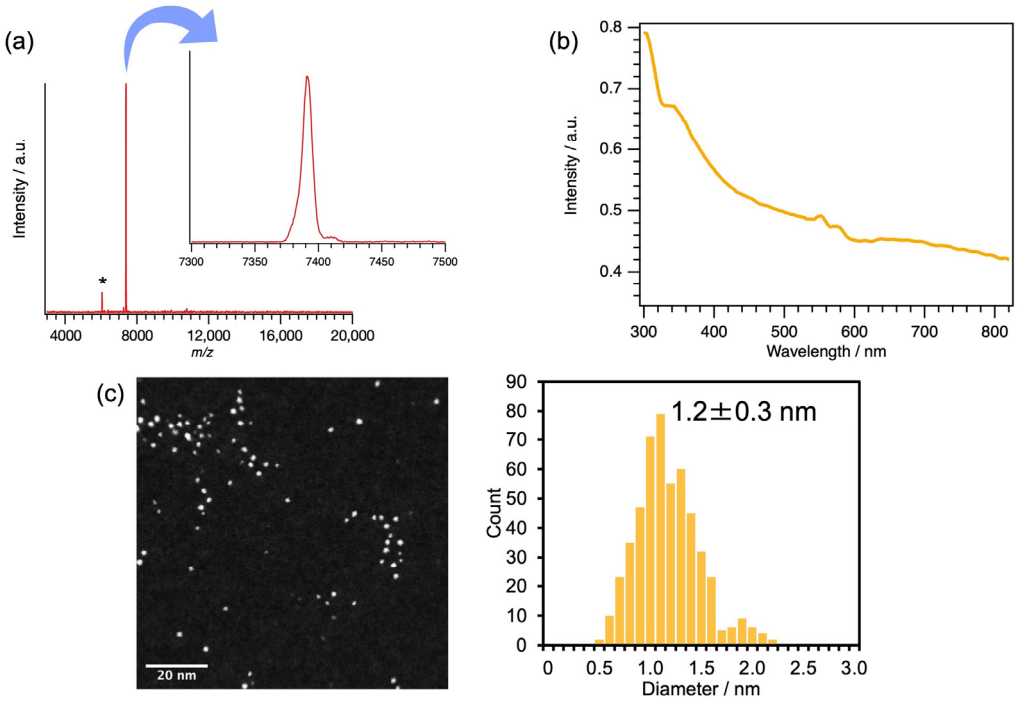

Figure 2. Characterization of the $Au_{25}PET_{18}$. (**a**) MALDI-TOF-MS spectra (* is a fragment peak), (**b**) UV-Vis absorption spectrum and (**c**) a STEM image and the particle size distribution of the $Au_{25}PET_{18}$ sample.

Size distribution and elemental analysis of the synthesized clusters were performed by STEM/EDS measurements (Figures 2c and S3). The estimated size was 1.2 ± 0.3 nm, close to the longest interatomic distance of 11.99 Å observed by single-crystal analysis reported in the previous paper [31]. EDS mapping also indicates that Au and S are present in the same particle. XPS measurement was conducted with tetraoctylammonium bromide (TOAB) which was added to the solution before casting on highly oriented pyrolytic graphene (HOPG) (Figure S4). The observed peaks of Au 4f, which show higher binding energy than that of bulk Au, suggested the successful formation of the Au_{25} superatom [29].

2.2. Comparison with Existing Methods

In the previous cases, thiol protected Au clusters were generally synthesized by reducing multimeric Au-thiol complexes [30,40,41]. In these methods, only the most stable species were obtained by the etching process after forming large Au clusters. In contrast, the Au cluster was synthesized directly through the collecting process of $AuCl_3$ to the dendrimer in this method (Figure 1). Therefore, the cluster formation speed is different from the previous cases [41]. MALDI-TOF-MS spectra confirmed the direct synthesis process (Figures 3a and S5). The intense peak corresponding to $Au_{25}PET_{18}$ (m/z = 7390.73) was generated within 15 min without peaks of large Au clusters. This result suggests that the assembly process on the TPM G4 is directly responsible for the Au_{25} nucleation. After one day of reaction, the main peak was still detectable; however, the peaks of degraded clusters also appeared. Therefore, it was appropriate to control the reaction time within a few hours of synthesis using the TPM G4.

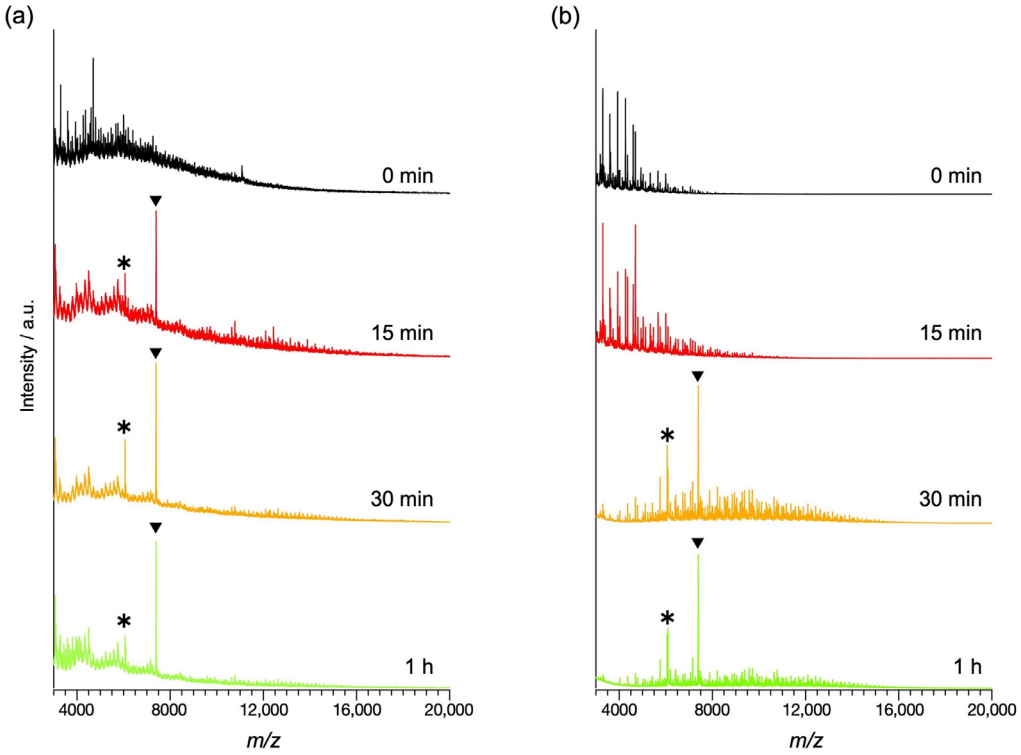

Figure 3. MALDI-TOF-MS spectra during $Au_{25}PET_{18}$ synthesis (**a**) with TPM G4 and (**b**) without TPM G4. ▼ are the peaks of $Au_{25}PET_{18}$, and * is the fragment peaks.

The same synthetic procedure was carried out without the dendrimer (Figure S6). This method also shows the formation of $Au_{25}PET_{18}$ after a reaction time of about 30 min (Figures 3b and S7). This reaction time is considered to be derived from the etching process of the nanoparticles to the Au_{25} superatom by the ligands.

These differences in the formation process can be seen in the appearance of the solutions (Figure S8). When the dendrimer (TPM G4) was used, the color of the solution changed from red (0 min) [41] (the early stage of $Au_{25}PET_{18}$ synthesis) to brown (after 2 min) (color of $Au_{25}PET_{18}$). The color was maintained for 12 h. On the other hand, in the case without the TPM G4, the solution turned black at 0 min immediately after the reduction and remained grayish at 15 min. After 11 h, the formation of the $Au_{25}PET_{18}$ was suggested by the color of the solution; however, the solution contained a black precipitate, indicating the formation of large particles. In the case of the dendrimer (Figure 3a), several peaks with small intensity are also observed in the range of m/z = 3000–7500 at 15 min after reduction. These peaks are considered to be the small Au-thiol multimer and decomposed products of the TPM G4 (Figure S9).

2.3. Synthesis of $MAu_{24}PET_{18}$ Using the Dendrimer TPM G4 as a Template

The advantage of the TPM G4 includes metal blending ability. Here, we investigated the blending of metals using the TPM G4. In the case of previous methods, the introduction of other metals using the ligand effect was reported [20,24,27,28,36–39,78]. The blending of metals was conducted using the complexation process (Figure 4a). In this synthesis, one equivalent of $Pd(CH_3CN)_4(BF_4)_2$ and 24 equivalents of $AuCl_3$ were coordinated to the dendrimer, and the thiol was added simultaneously with the reduction (Figure 4a). The formation of $PdAu_{24}PET_{18}$ was confirmed in the MALDI-TOF-MS spectrum (Figure 4b). The structure of the $PdAu_{24}PET_{18}$ was previously proposed as a Pd encapsulated structure (Figure S10). The MALDI-TOF-MS spectra show the formation of not only $PdAu_{24}PET_{18}$ but also $Au_{25}PET_{18}$. In fact, $Au_{25}PET_{18}$ was observed as a strong peak, and the intensity of $PdAu_{24}PET_{18}$ was about 1/13 of that of $Au_{25}PET_{18}$ This result suggests the partial

reconstruction of the stable $Au_{25}PET_{18}$ structure. STEM/EDS analysis of the prepared particles confirmed the presence of Pd and Au on the same particle (Figure S11).

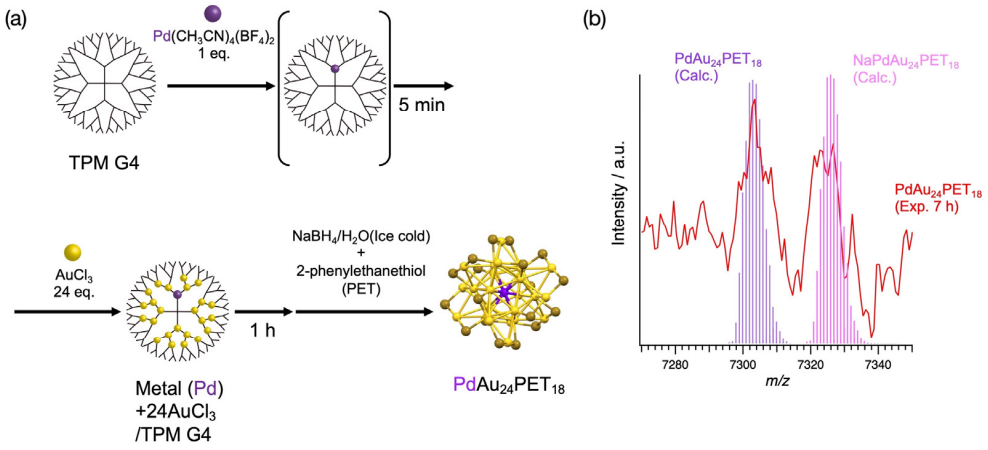

Figure 4. (**a**) Synthetic scheme of thiol-protected Au clusters blended with different elements (Pd) and (**b**) MALDI-TOF-MS spectrum of $PdAu_{24}PET_{18}$.

In the case of Pt introduction, the presence of Pt and Au on the same particle was confirmed by STEM/EDS analysis. However, the MALDI-TOF-MS spectra of the sample are not useful, unfortunately (Figure S12c). The observed peak at *m/z* = 7392 is close to that of $Au_{25}PET_{18}$; therefore, we could not determine the formation of $PtAu_{24}PET_{18}$ in the MS spectra. In this case, the comparison of the MS spectra is difficult since the masses of $PtAu_{24}PET_{18}$ (*m/z* = 7390.93) and $Au_{25}PET_{18}$ (*m/z* = 7391.93) are very close (Figure S14).

3. Materials and Methods

3.1. Chemicals

The TPM G4 (synthesized by the method [59] reported previously by our group), gold(III) chloride ($AuCl_3$, Sigma-Aldrich Japan, 99%), platinum(IV) chloride ($PtBr_4$, Thermo Scientific, 99.99+% (metals basis), Pt 57% min), tetrakis(acetonitrile)palladium(II) tetrafluoroborate ($Pd(CH_3CN)_4(BF_4)_2$, Sigma-Aldrich Japan), 2-phenylethanethiol ($HSC_2H_4C_6H_5$, Sigma-Aldrich Japan, 98%), sodium borohydride ($NaBH_4$, Kanto Chemical, >92.0% (T)), chloroform ($CHCl_3$, Fujifilm, for Organic Synthesis, 99.0+% (Capillary GC)), acetonitrile (CH_3CN, Kanto Chemical, Organics, >99.5% (GC)), toluene ($C_6H_5CH_3$, Kanto Chemical, Organics, >99.5% (GC)), ultrapure water (Merck Millipore, generated with Milli-Q Element A10, conductivity 18.2 MΩ cm), trans-2-[3-(4-tert-Butylphenyl)-2-methyl-2-propenylidene]malononitrile (DCTB, TCI, >98.0% (GC)) and Tetraoctylammonium bromide ($[CH_3(CH_2)_7]_4N(Br)$, TOAB, Sigma-Aldrich Japan, 98%) were used.

3.2. Assembly Accumulation of $AuCl_3$ on Dendrimer TPM G4

Solution preparation was performed in a glove box under a nitrogen atmosphere. First, $AuCl_3$ (22.7 mg, 74.7 μmol) was dissolved in acetonitrile to prepare a 2.99 mM solution. The dendrimer TPM G4 (0.380 mg, 34.4 nmol) was dissolved in chloroform and acetonitrile was added to prepare a 3.43 μM chloroform:acetonitrile = 1:1 solution. The complexation of $AuCl_3$ and the TPM G4 was monitored by a UV-Vis spectrometer.

3.3. Synthesis of $Au_{25}PET_{18}$ Using Dendrimers

$AuCl_3$ acetonitrile solution (10.4 mM, 25.0 mL) and the TPM G4 chloroform: acetonitrile = 1:1 solution (44.9 μM, 10.0mL) were prepared in a glove box under a nitrogen atmosphere. The TPM G4 solution was stirred for 1 h in the air under light-shielding conditions after the addition of 25 equivalents of the metal salt. After 1 h, ice-cold water with $NaBH_4$ (26.6 mg, 0.704 mmol, 1500 equivalents of the metal salt) and 2-phenylethanethiol

(10 μL, 74.5 μmol) were added for reduction and thiol protection. The amount of PET (Au:PET = 1:6) was determined based on a previous report [44]. The reaction was monitored by MALDI-TOF-MS.

After the addition of the reducing agent, the organic layer of the reaction solution was filtered. Then, the solution was concentrated using an evaporator. The obtained samples were washed several times with water/methanol. For STEM measurements, 1 μL of the sample solution (acetonitrile) was drop-casted onto a TEM grid (grid with carbon support film Super Hi-Res Carbon SHR-C075 STEM Cu75P grid, Okenshoji Co., Ltd., Tokyo, Japan). After the casting, the TEM grids were vacuum dried overnight. For XPS measurements, TOAB was added to the sample solution at 1.2 equivalents of Au. The solution was cast onto HOPG (490HP-AB HOPG SPI-3(ZYH) Grade 5 × 5 × 1 mm, Alliance Biosystems).

In this method, $Au_{25}PET_{18}$ can be synthesized by using a TPM G4 solution with concentrations of 9.29 μM–3.04 mM.

3.4. Synthesis of $MAu_{24}PET_{18}$ (M = Pd, Pt) Using Dendrimers

$AuCl_3$ (79.4 mg, 0.262 mmol) was dissolved in acetonitrile to prepare a solution of 10.5 mM; $Pd(CH_3CN)_4(BF_4)_2$ (15.4 mg, 34.7 μmol) was dissolved in acetonitrile to prepare a solution of 3.47 mM; $PtBr_4$ (18.8 mg, 36.4 μmol) was dissolved in acetonitrile to prepare a solution of 3.65 mM. The dendrimer TPM G4 (10.3 mg, 930 μmol) was dissolved in chloroform, and acetonitrile was added to prepare a 46.5 μM solution (chloroform:acetonitrile = 1:1). One equivalent of the metal salt of Pd or Pt was added to the dendrimer solution under atmospheric conditions and stirred for 5 min. Then, 24 equivalents of Au metal salt were added, and the mixture was stirred for 1 h under a light shield. After 1 h, ice-cold water containing $NaBH_4$ (54.9 mg, 1.45 mmol) and 2-phenylethanethiol (90 μL, 671 μmol) were added simultaneously to the dendrimer complex solution. The amount of 2-phenylethanethiol was determined based on a previous report [44]. The reaction was monitored by MALDI measurements.

3.5. Characterization

The UV-vis absorption spectra were obtained by Shimadzu UV-3150 and UV-3600 spectrometers. MALDI-TOF-MS spectra were obtained by Bruker microflex-YI, ultrafleXtreme. DCTB was used as the matrix, and toluene or chloroform was used as the solvent at a concentration of 20 mg/mL. The samples were mixed in 1:20 volume ratios. STEM measurements were carried out by a JEOL JEM-ARM200F equipped with an EDS analyzer (acceleration voltage: 80 kV). XPS measurements were carried out by ULVAC-PHI ESCA 1700R. The X-ray source was monochrome Al Kα (1486.7 eV). The neutralizer's emission current was 1 μA.

4. Conclusions

Dendrimer template synthesis of a Au_{25} superatom was developed with thiol protection. Unlike conventional synthetic methods, the conditions for synthesis are unique in that they do not require special conditions (e.g., low temperature reaction, a reaction in two separated aqueous and organic layers, or a long reaction time in the order of several days). The reduction and thiol coordination are performed for $AuCl_3$ in the TPM G4, resulting in a short-time synthesis. The addition of different elements using this method was also demonstrated by using Pd or Pt atoms.

Supplementary Materials: The following supporting information can be downloaded at: https://www.mdpi.com/article/10.3390/molecules27113398/s1, Figure S1. Schematic diagram of the structure and coordination of the dendrimer (TPM G4) used in this study. Figure S2. (**a**) Coordination image of $AuCl_3$ to TPM G4, (**b**) UV-Vis absorption spectra obtained by tightening of $AuCl_3$ vs. TPM G4, (**c**) magnified view of UV-Vis absorption spectrum near the isoabsorption point and (**d**) the change in absorbance at 287 nm. Figure S3. (**a**) STEM image, (**b**) STEM/EDS mapping image and (**c, d**) EDS spectrum (yellow: whole image, gray: blank area) of $Au_{25}PET_{18}$ XPS spectrum of $Au_{25}PET_{18}$ and Au wire. X-ray source is monochrome Al Kα (1486.7 eV). Neutralizer's emission

current is 1μA. Figure S5. MALDI-TOF-MS spectra after 2 h of the $Au_{25}PET_{18}$ synthesis reaction with TPM G4. Figure S6. Synthetic procedure of $Au_{25}PET_{18}$ cluster not using TPM G4. Note: main product is Au nanoparticle. The concentration of $AuCl_3$ was the same as when synthesized using TPM G4. In the presence of dendrimers, the equivalent of 25 equivalents of $AuCl_3$ is 45 μM. Figure S7. MALDI-TOF-MS spectra after 2 h of the $Au_{25}PET_{18}$ synthesis reaction without TPM G4. Figure S8. Comparison during synthesis of $Au_{25}PET_{18}$ with and without TPM G4. A significant color change is observed immediately after reduction. Figure S9. Image of the effect of dendrimer during $Au_{25}PET_{18}$ synthesis and its main and byproducts. Figure S10. The image of the stable structures of $PdAu_{24}PET_{18}$ (note: draw a figure with reference to the previous report [76]). Figure S11. (**a**) STEM image, (**b**) STEM/EDS mapping image and (**c**) EDS spectrum (purple: whole image, gray: blank area) of $PdAu_{24}PET_{18}$. Figure S12. (**a**) Synthetic scheme of thiol-protected Au clusters blended with different elements (Pt), (**b**) the image of the possible structures of $PtAu_{24}PET_{18}$ (note: draw a figure with reference to the previous report [20],), (**c**) MS spectrum of $PtAu_{24}SR_{18}$. Figure S13. (**a**) STEM image, (**b**) STEM/EDS mapping image and (c,d) EDS spectrum (light blue: whole image, gray: blank area) of $PtAu_{24}PET_{18}$. Figure S14. A comparison of the simulated values (light blue: $PtAu_{24}PET_{18}$ and yellow: $Au_{25}PET_{18}$) and the measured value of $PtAu_{24}PET_{18}$ (red).

Author Contributions: Conceptualization, H.M., T.K. and K.Y.; methodology, H.M., T.K. and K.Y.; validation, H.M. and T.K.; formal analysis, H.M. and T.K.; writing—original draft preparation, H.M. and T.K.; writing—review and editing, H.M. and T.K.; visualization, H.M.; supervision, K.Y., H.M., T.K., T.T., T.I. and K.Y. All authors have read and agreed to the published version of the manuscript.

Funding: This research was funded by JST ERATO Grant Number JPMJER1503, JSPS KAKENHI Grant Number 21H05023, 20K05538 and 22H04507, JST SPRING Grant Number JPMJSP2106, Canon Foundation and Five-star Alliance.

Institutional Review Board Statement: Not applicable.

Informed Consent Statement: Not applicable.

Data Availability Statement: The data generated and analyzed during the study are available in this article.

Acknowledgments: The authors thank Masato Koizumi, Materials Analysis Division, Open Facility Center, Tokyo Institute of Technology, for MALDI-TOF-MS analysis. This work was partially supported by the Tokyo Tech Academy for Convergence of Materials and Informatics (TAC-MI).

Conflicts of Interest: The authors declare no conflict of interest.

Sample Availability: Samples of the compounds are available from the authors upon request.

References

1. Tsukamoto, T.; Haruta, N.; Kambe, T.; Kuzume, A.; Yamamoto, K. Periodicity of Molecular Clusters Based on Symmetry-Adapted Orbital Model. *Nat. Commun.* **2019**, *10*, 3727. [CrossRef] [PubMed]
2. Ekardt, W. Dynamical polarizability of small metal particles: Self-consistent spherical jellium background model. *Phys. Rev. Lett.* **1984**, *52*, 1925–1928. [CrossRef]
3. Leuchtner, R.E.; Harms, A.C.; Castleman, A.W. Thermal metal cluster anion reactions: Behavior of aluminum clusters with oxygen. *J. Chem. Phys.* **1989**, *91*, 2753–2754. [CrossRef]
4. Luo, Z.; Berkdemir, C.; Smith, J.C.; Castleman, A.W. Cluster reaction of $[Ag_8]^-$/$[Cu_8]^-$ with chlorine: Evidence for the harpoon mechanism? *Chem. Phys. Lett.* **2013**, *582*, 24–30. [CrossRef]
5. Brust, M.; Walker, M.; Bethell, D.; Schiffrin, D.J.; Whyman, R. Synthesis of thiol-derivatised gold nanoparticles in a two-phase liquid–liquid system. *J. Chem. Soc. Chem. Commun.* **1994**, *7*, 801–802. [CrossRef]
6. Chaki, N.K.; Negishi, Y.; Tsunoyama, H.; Shichibu, Y.; Tsukuda, T. Ubiquitous 8 and 29 KDa gold: Alkanethiolate cluster compounds: Mass-spectrometric determination of molecular formulas and structural implications. *J. Am. Chem. Soc.* **2008**, *130*, 8608–8610. [CrossRef]
7. Kimura, K.; Sugimoto, N.; Sato, S.; Yao, H.; Negishi, Y.; Tsukuda, T. Size determination of gold clusters by polyacrylamide gel electrophoresis in a large cluster region. *J. Phys. Chem. C* **2009**, *113*, 14076–14082. [CrossRef]
8. Xie, S.; Tsunoyama, H.; Kurashige, W.; Negishi, Y.; Tsukuda, T. Enhancement in aerobic alcohol oxidation catalysis of Au_{25} clusters by single Pd atom doping. *ACS Catal.* **2012**, *2*, 1519–1523. [CrossRef]
9. Negishi, Y.; Chaki, N.K.; Shichibu, Y.; Whetten, R.L.; Tsukuda, T. Origin of magic stability of thiolated gold clusters: A case study on $Au_{25}(SC_6H_{13})_{18}$. *J. Am. Chem. Soc.* **2007**, *129*, 11322–11323. [CrossRef]

10. Negishi, Y.; Takasugi, Y.; Sato, S.; Yao, H.; Kimura, K.; Tsukuda, T. Magic-numbered Au_n clusters protected by glutathione monolayers (n = 18, 21, 25, 28, 32, 39): Isolation and spectroscopic characterization. *J. Am. Chem. Soc.* **2004**, *126*, 6518–6519. [CrossRef]
11. Negishi, Y.; Takasugi, Y.; Sato, S.; Yao, H.; Kimura, K.; Tsukuda, T. Kinetic stabilization of growing gold clusters by passivation with thiolates. *J. Phys. Chem. B* **2006**, *110*, 12218–12221. [CrossRef] [PubMed]
12. Yamazoe, S.; Kurashige, W.; Nobusada, K.; Negishi, Y.; Tsukuda, T. Preferential location of coinage metal dopants (M = Ag or Cu) in $[Au_{25-x}M_x(SC_2H_4Ph)_{18}]^-$ ($x \sim 1$) as determined by extended X-ray absorption fine structure and density functional theory calculations. *J. Phys. Chem. C* **2014**, *118*, 25284–25290. [CrossRef]
13. Negishi, Y.; Nakazaki, T.; Malola, S.; Takano, S.; Niihori, Y.; Kurashige, W.; Yamazoe, S.; Tsukuda, T.; Häkkinen, H. A critical size for emergence of nonbulk electronic and geometric structures in dodecanethiolate-protected Au clusters. *J. Am. Chem. Soc.* **2015**, *137*, 1206–1212. [CrossRef] [PubMed]
14. Sharma, S.; Yamazoe, S.; Ono, T.; Kurashige, W.; Niihori, Y.; Nobusada, K.; Tsukuda, T.; Negishi, Y. Tuning the electronic structure of thiolate-protected 25-atom clusters by co-substitution with metals having different preferential sites. *Dalton Trans.* **2016**, *45*, 18064–18068. [CrossRef] [PubMed]
15. Hirata, K.; Yamashita, K.; Muramatsu, S.; Takano, S.; Ohshimo, K.; Azuma, T.; Nakanishi, R.; Nagata, T.; Yamazoe, S.; Koyasu, K.; et al. Anion photoelectron spectroscopy of free $[Au_{25}(SC_{12}H_{25})_{18}]^-$. *Nanoscale* **2017**, *9*, 13409–13412. [CrossRef] [PubMed]
16. Omoda, T.; Takano, S.; Tsukuda, T. Toward controlling the electronic structures of chemically modified superatoms of gold and silver. *Small* **2021**, *17*, 2001439. [CrossRef] [PubMed]
17. Hirata, K.; Kim, K.; Nakamura, K.; Kitazawa, H.; Hayashi, S.; Koyasu, K.; Tsukuda, T. Photoinduced thermionic emission from $[M_{25}(SR)_{18}]^-$ (M = Au, Ag) revealed by anion photoelectron spectroscopy. *J. Phys. Chem. C* **2019**, *123*, 13174–13179. [CrossRef]
18. Omoda, T.; Takano, S.; Tsukuda, T. Reduction-resistant $[Au_{25}(Cyclohexanethiolate)_{18}]^0$ with an icosahedral Au_{13} core. *Chem. Lett.* **2019**, *48*, 885–887. [CrossRef]
19. Suyama, M.; Takano, S.; Nakamura, T.; Tsukuda, T. Stoichiometric formation of open-shell $[PtAu_{24}(SC_2H_4Ph)_{18}]^-$ via spontaneous electron proportionation between $[PtAu_{24}(SC_2H_4Ph)_{18}]^{2-}$ and $[PtAu_{24}(SC_2H_4Ph)_{18}]^0$. *J. Am. Chem. Soc.* **2019**, *141*, 14048–14051. [CrossRef]
20. Suyama, M.; Takano, S.; Tsukuda, T. Synergistic effects of Pt and Cd Codoping to icosahedral Au_{13} superatoms. *J. Phys. Chem. C* **2020**, *124*, 23923–23929. [CrossRef]
21. Negishi, Y.; Kurashige, W.; Niihori, Y.; Nobusada, K. Toward the creation of stable, functionalized metal clusters. *Phys. Chem. Chem. Phys.* **2013**, *15*, 18736. [CrossRef] [PubMed]
22. Niihori, Y.; Koyama, Y.; Watanabe, S.; Hashimoto, S.; Hossain, S.; Nair, L.V.; Kumar, B.; Kurashige, W.; Negishi, Y. Atomic and isomeric separation of thiolate-protected alloy clusters. *J. Phys. Chem. Lett.* **2018**, *9*, 4930–4934. [CrossRef] [PubMed]
23. Hossain, S.; Niihori, Y.; Nair, L.V.; Kumar, B.; Kurashige, W.; Negishi, Y. Alloy clusters: Precise synthesis and mixing effects. *Acc. Chem. Res.* **2018**, *51*, 3114–3124. [CrossRef] [PubMed]
24. Sharma, S.; Kurashige, W.; Nobusada, K.; Negishi, Y. Effect of trimetallization in thiolate-protected $Au_{24-n}Cu_nPd$ clusters. *Nanoscale* **2015**, *7*, 10606–10612. [CrossRef] [PubMed]
25. Negishi, Y.; Kurashige, W.; Niihori, Y.; Iwasa, T.; Nobusada, K. Isolation, structure, and stability of a dodecanethiolate-protected Pd1Au24 cluster. *Phys. Chem. Chem. Phys.* **2010**, *12*, 6219. [CrossRef]
26. Hossain, S.; Suzuki, D.; Iwasa, T.; Kaneko, R.; Suzuki, T.; Miyajima, S.; Iwamatsu, Y.; Pollitt, S.; Kawawaki, T.; Barrabés, N.; et al. Determining and controlling Cu-substitution sites in thiolate-protected gold-based 25-atom alloy nanoclusters. *J. Phys. Chem. C* **2020**, *124*, 22304–22313. [CrossRef]
27. Negishi, Y.; Iwai, T.; Ide, M. Continuous modulation of electronic structure of stable thiolate-protected Au25 cluster by Ag doping. *Chem. Commun.* **2010**, *46*, 4713. [CrossRef]
28. Negishi, Y.; Munakata, K.; Ohgake, W.; Nobusada, K. Effect of copper doping on electronic structure, geometric structure, and stability of thiolate-protected Au_{25} nanoclusters. *J. Phys. Chem. Lett.* **2012**, *3*, 2209–2214. [CrossRef]
29. Ohta, T.; Shibuta, M.; Tsunoyama, H.; Negishi, Y.; Eguchi, T.; Nakajima, A. Size and structure dependence of electronic states in thiolate-protected gold nanoclusters of $Au_{25}(SR)_{18}$, $Au_{38}(SR)_{24}$, and $Au_{144}(SR)_{60}$. *J. Phys. Chem. C* **2013**, *117*, 3674–3679. [CrossRef]
30. Zhu, M.; Aikens, C.M.; Hollander, F.J.; Schatz, G.C.; Jin, R. Correlating the crystal structure of a thiol-protected Au_{25} cluster and optical properties. *J. Am. Chem. Soc.* **2008**, *130*, 5883–5885. [CrossRef]
31. Heaven, M.W.; Dass, A.; White, P.S.; Holt, K.M.; Murray, R.W. Crystal structure of the gold nanoparticle $[N(C_8H_{17})_4][Au_{25}(SCH_2CH_2Ph)_{18}]$. *J. Am. Chem. Soc.* **2008**, *130*, 3754–3755. [CrossRef] [PubMed]
32. Dolamic, I.; Knoppe, S.; Dass, A.; Bürgi, T. First enantioseparation and circular dichroism spectra of Au38 clusters protected by achiral ligands. *Nat. Commun.* **2012**, *3*, 798. [CrossRef] [PubMed]
33. Qian, H.; Eckenhoff, W.T.; Zhu, Y.; Pintauer, T.; Jin, R. Total structure determination of thiolate-protected Au_{38} nanoparticles. *J. Am. Chem. Soc.* **2010**, *132*, 8280–8281. [CrossRef] [PubMed]
34. Bahena, D.; Bhattarai, N.; Santiago, U.; Tlahuice, A.; Ponce, A.; Bach, S.B.H.; Yoon, B.; Whetten, R.L.; Landman, U.; Jose-Yacaman, M. STEM electron diffraction and high-resolution images used in the determination of the crystal structure of the $Au_{144}(SR)_{60}$ cluster. *J. Phys. Chem. Lett.* **2013**, *4*, 975–981. [CrossRef] [PubMed]

35. Malola, S.; Lehtovaara, L.; Enkovaara, J.; Häkkinen, H. Birth of the localized surface plasmon resonance in monolayer-protected gold nanoclusters. *ACS Nano* **2013**, *7*, 10263–10270. [CrossRef] [PubMed]
36. Qian, H.; Jiang, D.; Li, G.; Gayathri, C.; Das, A.; Gil, R.R.; Jin, R. Monoplatinum doping of gold nanoclusters and catalytic application. *J. Am. Chem. Soc.* **2012**, *134*, 16159–16162. [CrossRef] [PubMed]
37. Christensen, S.L.; MacDonald, M.A.; Chatt, A.; Zhang, P.; Qian, H.; Jin, R. Dopant location, local structure, and electronic properties of $Au_{24}Pt(SR)_{18}$ nanoclusters. *J. Phys. Chem. C* **2012**, *116*, 26932–26937. [CrossRef]
38. Wang, S.; Song, Y.; Jin, S.; Liu, X.; Zhang, J.; Pei, Y.; Meng, X.; Chen, M.; Li, P.; Zhu, M. Metal exchange method using Au_{25} nanoclusters as templates for alloy nanoclusters with atomic precision. *J. Am. Chem. Soc.* **2015**, *137*, 4018–4021. [CrossRef]
39. Yang, S.; Wang, S.; Jin, S.; Chen, S.; Sheng, H.; Zhu, M. A metal exchange method for thiolate-protected tri-metal $M_1Ag_xAu_{24-x}(SR)_{18}{}^0$ (M = Cd/Hg) nanoclusters. *Nanoscale* **2015**, *7*, 10005–10007. [CrossRef]
40. Zhu, M.; Lanni, E.; Garg, N.; Bier, M.E.; Jin, R. Kinetically controlled, high-yield synthesis of Au $_{25}$ clusters. *J. Am. Chem. Soc.* **2008**, *130*, 1138–1139. [CrossRef]
41. Dharmaratne, A.C.; Krick, T.; Dass, A. Nanocluster size evolution studied by mass spectrometry in room temperature $Au_{25}(SR)_{18}$ synthesis. *J. Am. Chem. Soc.* **2009**, *131*, 13604–13605. [CrossRef] [PubMed]
42. Esumi, K.; Miyamoto, K.; Yoshimura, T. Comparison of PAMAM–Au and PPI–Au nanocomposites and their catalytic activity for reduction of 4-nitrophenol. *J. Colloid Interface Sci.* **2002**, *254*, 402–405. [CrossRef] [PubMed]
43. Ye, H.; Crooks, R.M. Electrocatalytic O_2 reduction at glassy carbon electrodes modified with dendrimer-encapsulated Pt nanoparticles. *J. Am. Chem. Soc.* **2005**, *127*, 4930–4934. [CrossRef] [PubMed]
44. Ornelas, C.; Aranzaes, J.R.; Salmon, L.; Astruc, D. "Click" dendrimers: Synthesis, redox sensing of $Pd(OAc)_2$, and remarkable catalytic hydrogenation activity of precise Pd nanoparticles stabilized by 1,2,3-triazole-containing dendrimers. *Chem. Eur. J.* **2008**, *14*, 50–64. [CrossRef]
45. Garcia-Martinez, J.C.; Crooks, R.M. Extraction of Au nanoparticles having narrow size distributions from within dendrimer templates. *J. Am. Chem. Soc.* **2004**, *126*, 16170–16178. [CrossRef]
46. Kéki, S.; Török, J.; Deák, G.; Daróczi, L.; Zsuga, M. Silver nanoparticles by PAMAM-assisted photochemical reduction of Ag^+. *J. Colloid Interface Sci.* **2000**, *229*, 550–553. [CrossRef]
47. Ostojic, N.; Duan, Z.; Galyamova, A.; Henkelman, G.; Crooks, R.M. Electrocatalytic study of the oxygen reduction reaction at gold nanoparticles in the absence and presence of interactions with SnO_x supports. *J. Am. Chem. Soc.* **2018**, *140*, 13775–13785. [CrossRef]
48. Hayakawa, K.; Yoshimura, T.; Esumi, K. Preparation of gold−dendrimer nanocomposites by laser irradiation and their catalytic reduction of 4-nitrophenol. *Langmuir* **2003**, *19*, 5517–5521. [CrossRef]
49. Esumi, K.; Suzuki, A.; Aihara, N.; Usui, K.; Torigoe, K. Preparation of gold colloids with UV irradiation using dendrimers as stabilizer. *Langmuir* **1998**, *14*, 3157–3159. [CrossRef]
50. Boisselier, E.; Diallo, A.K.; Salmon, L.; Ornelas, C.; Ruiz, J.; Astruc, D. Encapsulation and stabilization of gold nanoparticles with "click" polyethyleneglycol dendrimers. *J. Am. Chem. Soc.* **2010**, *132*, 2729–2742. [CrossRef]
51. Ispasoiu, R.G.; Balogh, L.; Varnavski, O.P.; Tomalia, D.A. Goodson large optical limiting from novel metal–dendrimer nanocomposite materials. *J. Am. Chem. Soc.* **2000**, *122*, 11005–11006. [CrossRef]
52. Esumi, K.; Suzuki, A.; Yamahira, A.; Torigoe, K. Role of poly(amidoamine) dendrimers for preparing nanoparticles of gold, platinum, and silver. *Langmuir* **2000**, *16*, 2604–2608. [CrossRef]
53. Ottaviani, M.F.; Montalti, F.; Turro, N.J.; Tomalia, D.A. Characterization of starburst dendrimers by the EPR technique. Copper(II) ions binding full-generation dendrimers. *J. Phys. Chem. B* **1997**, *101*, 158–166. [CrossRef]
54. Ottaviani, M.F.; Bossmann, S.; Turro, N.J.; Tomalia, D.A. Characterization of starburst dendrimers by the EPR technique. 1. Copper complexes in water solution. *J. Am. Chem. Soc.* **1994**, *116*, 661–671. [CrossRef]
55. He, J.-A.; Valluzzi, R.; Yang, K.; Dolukhanyan, T.; Sung, C.; Kumar, J.; Tripathy, S.K.; Samuelson, L.; Balogh, L.; Tomalia, D.A. Electrostatic multilayer deposition of a gold−dendrimer nanocomposite. *Chem. Mater.* **1999**, *11*, 3268–3274. [CrossRef]
56. Balogh, L.; Valluzzi, R.; Laverdure, K.S.; Gido, S.P.; Hagnauer, G.L.; Tomalia, D.A. Formation of silver and gold dendrimer nanocomposites. *J. Nanopart. Res.* **1999**, *1*, 353–368. [CrossRef]
57. Balogh, L.; Tomalia, D.A. Poly(amidoamine) dendrimer-templated nanocomposites. 1. Synthesis of zerovalent copper nanoclusters. *J. Am. Chem. Soc.* **1998**, *120*, 7355–7356. [CrossRef]
58. Zhao, M.; Sun, L.; Crooks, R.M. Preparation of Cu nanoclusters within dendrimer templates. *J. Am. Chem. Soc.* **1998**, *120*, 4877–4878. [CrossRef]
59. Enoki, O.; Katoh, H.; Yamamoto, K. Synthesis and properties of a novel phenylazomethine dendrimer with a tetraphenylmethane core. *Org. Lett.* **2006**, *8*, 569–571. [CrossRef]
60. Yamamoto, K.; Higuchi, M.; Shiki, S.; Tsuruta, M.; Chiba, H. Stepwise radial complexation of imine groups in phenylazomethine dendrimers. *Nature* **2002**, *415*, 509–511. [CrossRef]
61. Takanashi, K.; Fujii, A.; Nakajima, R.; Chiba, H.; Higuchi, M.; Einaga, Y.; Yamamoto, K. Heterometal assembly in dendritic polyphenylazomethines. *Bull. Chem. Soc. Jpn.* **2007**, *80*, 1563–1572. [CrossRef]
62. Yamamoto, K.; Imaoka, T.; Chun, W.-J.; Enoki, O.; Katoh, H.; Takenaga, M.; Sonoi, A. Size-specific catalytic activity of platinum clusters enhances oxygen reduction reactions. *Nat. Chem.* **2009**, *1*, 397–402. [CrossRef] [PubMed]

63. Kambe, T.; Imaoka, S.; Imaoka, T.; Yamamoto, K. Build-up enhancement of photoluminescence from phenylazomethine bismuth dendrimer using Bi(OTf)3. *J. Nanopart. Res.* **2018**, *20*, 118. [CrossRef]
64. Kambe, T.; Watanabe, A.; Imaoka, T.; Yamamoto, K. Bismuth complexes in phenylazomethine dendrimers: Controllable luminescence and emission in the solid state. *Angew. Chem. Int. Ed.* **2016**, *55*, 13151–13154. [CrossRef] [PubMed]
65. Imaoka, T.; Fushimi, M.; Kimoto, A.; Okamoto, Y.; Takanashi, K.; Yamamoto, K. Resistive switching memory based on size-controlled 1-nm gold particles. *Chem. Lett.* **2014**, *43*, 1269–1271. [CrossRef]
66. Takahashi, M.; Koizumi, H.; Chun, W.-J.; Kori, M.; Imaoka, T.; Yamamoto, K. Finely controlled multimetallic nanocluster catalysts for solvent-free aerobic oxidation of hydrocarbons. *Sci. Adv.* **2017**, *3*, e1700101. [CrossRef]
67. Tsukamoto, T.; Kambe, T.; Nakao, A.; Imaoka, T.; Yamamoto, K. Atom-hybridization for synthesis of polymetallic clusters. *Nat. Commun.* **2018**, *9*, 3873. [CrossRef]
68. Kambe, T.; Li, M.; Tsukamoto, T.; Imaoka, T.; Yamamoto, K. Expansion of Dendrimer Template Function for Subnanoparticle Synthesis. *Chem. Lett.* **2021**, *50*, 1648–1651. [CrossRef]
69. Kambe, T.; Yamamoto, K. Functionalization of Phenylazomethine Dendrimers. *Polym J* **2022**, *54*, 97–105. [CrossRef]
70. Imaoka, T.; Kitazawa, H.; Chun, W.; Yamamoto, K. Finding the most catalytically active platinum clusters with low atomicity. *Angew. Chem. Int. Ed.* **2015**, *54*, 9810–9815. [CrossRef]
71. Kambe, T.; Haruta, N.; Imaoka, T.; Yamamoto, K. Solution-phase synthesis of Al_{13}^- using a dendrimer template. *Nat. Commun.* **2017**, *8*, 2046. [CrossRef] [PubMed]
72. Kambe, T.; Watanabe, A.; Li, M.; Tsukamoto, T.; Imaoka, T.; Yamamoto, K. Superatomic gallium clusters in dendrimers: Unique Rigidity and reactivity depending on their atomicity. *Adv. Mater.* **2020**, *32*, 1907167. [CrossRef] [PubMed]
73. Dass, A.; Stevenson, A.; Dubay, G.R.; Tracy, J.B.; Murray, R.W. Nanoparticle MALDI-TOF mass spectrometry without fragmentation: $Au_{25}(SCH_2CH_2Ph)_{18}$ and mixed monolayer $Au_{25}(SCH_2CH_2Ph)_{18-x}(L)_x$. *J. Am. Chem. Soc.* **2008**, *130*, 5940–5946. [CrossRef] [PubMed]
74. Patiny, L.; Borel, A. ChemCalc: A building block for tomorrow's chemical infrastructure. *J. Chem. Inf. Model.* **2013**, *53*, 1223–1228. [CrossRef] [PubMed]
75. Shichibu, Y.; Negishi, Y.; Tsukuda, T.; Teranishi, T. Large-scale synthesis of thiolated Au_{25} clusters via ligand exchange reactions of phosphine-stabilized Au_{11} clusters. *J. Am. Chem. Soc.* **2005**, *127*, 13464–13465. [CrossRef]
76. Tracy, J.B.; Kalyuzhny, G.; Crowe, M.C.; Balasubramanian, R.; Choi, J.-P.; Murray, R.W. Poly(ethylene glycol) ligands for high-resolution nanoparticle mass spectrometry. *J. Am. Chem. Soc.* **2007**, *129*, 6706–6707. [CrossRef]
77. Donkers, R.L.; Lee, D.; Murray, R.W. Synthesis and isolation of the molecule-like cluster $Au_{38}(PhCH_2CH_2S)_{24}$. *Langmuir* **2004**, *20*, 1945–1952. [CrossRef]
78. Tofanelli, M.A.; Ni, T.W.; Phillips, B.D.; Ackerson, C.J. Crystal structure of the $PdAu_{24}(SR)_{18}^0$ superatom. *Inorg. Chem.* **2016**, *55*, 999–1001. [CrossRef]